Korean J. Chem. Eng., **26**(3), 895-901 (2009)

Effect of pyrolysis temperature on the char micro-structure and reactivity of NO reduction

Yanshan Yin, Jun Zhang, and Changdong Sheng†

School of Energy & Environment, Southeast University, Si Pai Lou No.2, Nanjing 210096, P. R. China
(*Received 31 July 2008 • accepted 18 November 2008*)

Abstract−A phenol-formaldehyde resin (PFR) and a bituminous coal (SH) were pyrolyzed at various temperatures. The structure and the char-NO reactivity were analyzed in order to examine the effect of pyrolysis temperature on the micro-structure of the resulting char and further on the reactivity towards NO. Micro-structure of the char samples was characterized by Fourier transform infrared spectroscopy (FTIR), X-ray diffraction (XRD) and Raman spectroscopy. It was indicated that the micro-structure of PFR char and coal char experienced remarkable changes during pyrolysis, which resulted in the decrease of phenolic OH, aromatic hydrogen and more ordered structure. The pyrolysis temperature showed a weak impact on the reactivity of PFR char but comparatively remarkable impact on that of coal char at lower reaction temperature. Mineral matter in coal char presented a weak effect on the reactivity.

Key words: Pyrolysis, Char, Micro-structure, C-NO Reactivity

INTRODUCTION

NO is a well-known combustion-related pollutant causing photochemical smog and acid rain, which motivates extensive research efforts for reducing its emissions [1-3]. It has been proved that NO can be chemisorbed on the surface of carbon at lower temperature and react with carbon at higher temperature. Reduction of NO with carbonaceous materials with or without catalyst loading has been proposed as a promising way to lower NO emissions from combustion systems [4-13]. Among various carbonaceous materials, e.g., coal char, activated carbon, graphite, phenol-formaldehyde resin (PFR) char and biomass char, PFR char is an excellent model material used for the studies on the reduction of NO because it has a similar structure as coal char but negligible inorganic matter content [4-7,10].

Char-NO reaction is a typical heterogeneous reaction. The precursor of char, the presence of catalyst, pore structure, reaction temperature, reactant concentration and gas composition have impacts on the reaction rate [4-11]. Furthermore, heat treatment conditions during char preparation including pyrolysis temperature, heating rate and treatment time, to some degree, determine the element content, pore structure and micro-structure of resulting char and consequently influence gasification reactivity towards O_2 and CO_2 [14-16]. For NO-carbon gasification reaction, the reactivity of coal char towards NO was found to decrease with increasing pyrolysis temperature and soaking time [4,5]. Increasing heating rate during the char pyrolysis resulted in higher pore volume and total surface area and thus enhanced the rate of NO reduction [17]. According to Garcia-Garcia et al. [18], free reactive sites on char surface were created by C(O) complexes desorption and higher heat treatment temperature led to lower C(O) complexes content and thus lower reactivity towards NO. In addition, the results in Ref [19] indicated that the relative concentration of active sites depended on the structure of carbonaceous materials and NO-C reaction was a structure sensitive reaction. Although many studies including those mentioned above have been devoted to the effect of heat treatment conditions and pore structure on the NO reduction reactivity of various carbonaceous materials, few studies have addressed the influence of carbon chemical structure. Further research work is needed to understand the effect of micro-structure of char on the reactivity towards NO.

In this study, two carbonaceous materials including PFR and a bituminous coal were pyrolyzed at various temperatures. The resulting chars were characterized with Fourier transform infrared spectrometry (FTIR), X-ray diffraction (XRD) and Raman spectroscopy. FTIR is a useful technique to characterize the variations of functional groups in carbonization, coalification or oxidation process [20-24]. Non-destructive and quantitative techniques, XRD and Raman spectroscopy, are widely applied to characterize crystalline structure and/or molecular structure [25-33]. The three techniques were used to take a comprehensive characterization of the structure of PFR char. The NO gasification reactivity of the chars was measured by thermogravimetric analysis (TGA) under isothermal condition. The study was focused on the influence of pyrolysis temperature on the micro-structure of resulting chars and further on the gasification reactivity towards NO.

EXPERIMENTAL

1. Char Preparation

PFR and a bituminous coal (SH) were used as raw materials for char preparation. About 10 g PFR sample held in a ceramic boat was pyrolyzed in a tube furnace (i.d. 80 mm and length of 350 mm) under N_2 atmosphere at final temperature of 500, 600, 700, 800 and 900 °C. About 10 g coal sample was pyrolyzed in the tube furnace under high purity Ar atmosphere (99.999%) at final temperature of 500, 700 and 900 °C. To examine the influence of mineral matter, a small amount of the coal sample was subjected to acid washing to remove the inorganic matter following the procedure in Ref. [30].

†To whom correspondence should be addressed.
E-mail: c.d.sheng@seu.edu.cn
‡This paper was presented at the 7th China-Korea Workshop on Clean Energy Technology held at Taiyuan, China, June 26-28, 2008.

Table 1. Proximate and ultimate analyses of the materials studied

Proximate analysis: air dried basis (wt%)						
Sample	M	A	V	FC		
PFR	2.42	0	69.54	28.04		
SH coal	13.06	5.75	28.19	53.01		
Ultimate analysis: dry basis (wt%)						
	C	H	N	O*	H/C ratio	O/C ratio
SH-500	80.79	2.762	0.882	8.956	0.41	0.083
SH-700	83.04	1.302	0.469	8.579	0.19	0.077
SH-900	84.26	0.819	0.336	7.975	0.12	0.071
Dem-SH-500	85.41	2.679	0.614	11.297	0.38	0.099
Dem-SH-700	90.96	1.471	0.353	7.216	0.19	0.059
Dem-SH-900	94.46	0.763	0.285	4.492	0.10	0.036

* by difference

The demineralized coal sample (designated as Dem-SH) was also pyrolyzed under the same conditions as the parent coal sample. In the following section, the nomenclature of char is expressed as the name of the precursor followed by the pyrolysis temperature, e.g., PFR-500, SH-500 and Dem-SH-500. The proximate analysis and ultimate analysis of the raw materials and the char samples are presented in Table 1.

2. Characterization of Char Micro-structure

PFR chars were analyzed with an FTIR. The samples were prepared by forming standard KBr pellets for the FTIR analysis. FTIR spectra were recorded on a Bruker Vector 22 instrument from 400 to 4,000 cm^{-1} with a resolution of 4 cm^{-1}. Sixteen scans were made for each sample. The precision is no more than 0.01 cm^{-1}. For comparison purpose, Dem-SH and its chars were also characterized by FTIR analysis.

XRD analysis of PFR chars was performed with an ARL X'TRA X-ray diffractometer. Cu K_α radiation (45 kV, 35 mA) was used as the X-ray source (λ=0.1541 nm). Intensity was recorded from 5 to 100° with a scanning speed of 1°/min.

Laser Raman spectroscopy analysis was also performed on PFR chars with a Jobin Yvon Labram HR800 spectrometer. The laser power at the sample surface was fixed at about 1 mW, and the laser spot diameter reaching the sample was about 1 μm, much larger than the size of carbon micro-crystallites in the chars. Eight spectra were collected for each sample to obtain an average value. The spectra were recorded in the range of 800-2,000 cm^{-1}.

3. Reactivity Measurement in TGA

Isothermal reaction of PFR char, coal char and demineralized coal char was performed in Ar/NO (2.4% NO) atmosphere in a TGA (Setaram TGA92). The reaction temperature was in the range of 500 to 900 °C. About 10 mg char sample with particle size <105 μm was placed in the TGA pan. The sample was heated from room temperature to the preset reaction temperature under Ar atmosphere and then switched to Ar/NO atmosphere holding certain time, followed by stepwise increases in the temperature.

The rate of C-NO reaction under the isothermal condition can be expressed as

$$r = \frac{dX}{(1-X)dt} = kC_{NO}^{n} \quad (1)$$

$$X = \frac{m_0 - m}{m_0}, \quad k = A\exp(-E/RT) \quad (2)$$

where r is the global rate of the gasification reaction, X denotes the carbon conversion, and k is the rate constant. C_{NO} denotes NO concentration, and n is the reaction order.

RESULTS AND DISCUSSION

1. FTIR Analysis

The infrared (IR) spectrum in Fig. 1 reflects the evolutions of functional groups of the PFR chars, Dem-SH and its chars. Fig. 1 shows a wide band at 3,422-3,448 cm^{-1}, indicating the presence of intense phenolic OH stretching vibrations. The bands at 2,970, 2,922 and 2,852 cm^{-1} are due to symmetric CH_3 stretching, asymmetric CH_2 stretching and symmetric CH_2 stretching vibrations, respectively. The 1,719 cm^{-1} band is attributed to C=O groups. The assignment of 1,560-1,637 cm^{-1} band region is argued to be the aromatic ring stretching mode [21,22]. CH_2 bridges between aromatic rings

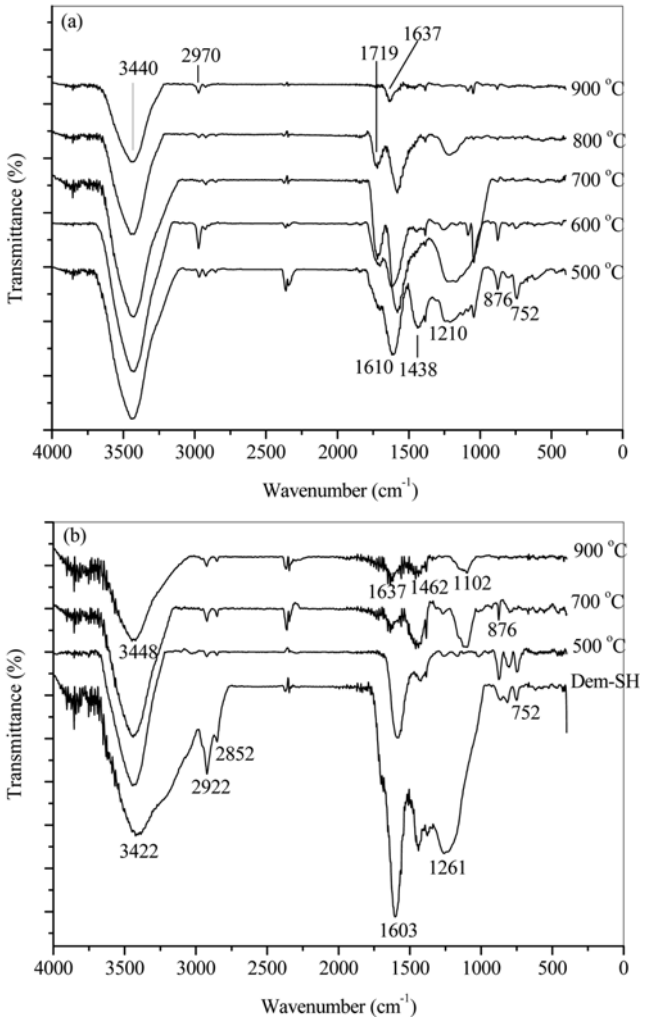

Fig. 1. FTIR spectra of (a) PFR chars and (b) demineralized coal and chars.

may be responsible for the band at 1,438-1,462 cm^{-1}. The bands at 1,210 and 1,261 cm^{-1} are due to ethers C-O stretching. The band at 1,064-1,102 cm^{-1}, which shows high intensity for the chars formed at higher pyrolysis temperature, is assigned to aromatic CH in-plane deformation vibrations. Both 876 and 752 cm^{-1} band represent the aromatic CH out-of-plane deformation vibrations. The former is due to substituted benzene rings with isolated H, and the latter denotes mono-substituted benzene rings and condensed ring [22].

It can be seen in Fig. 1 that both PFR chars and demineralized coal chars show a remarkable change of functional groups during pyrolysis. The intensities of hydroxyl groups (ca. 3,440 cm^{-1}) and aromatic hydrogen (900-700 cm^{-1}) decrease with increasing the pyrolysis temperature while the OH band shifts to higher wavenumber. As a result of the OH groups participating in the dehydration and cyclodehydration reactions, their intensities become gradually weaker with increasing the pyrolysis temperature. After being pyrolyzed at the temperatures of above 600 °C, CH_2 bridges of PFR char almost show negligible absorption peak, as shown in Fig. 1(a). The breakage of the CH_2 bridges causes the release of aliphatic carbon and some carbon orientation but not to graphitization under this pyrolysis condition [24]. The aromatic ring stretching in Fig. 1(a) and Fig. 1(b) as well as the C-O stretching in Fig. 1(b) also decrease with pyrolysis temperature. The decrease of C-O groups and the aromatic ring in the char during pyrolysis is attributed to the loss of polar substituted groups such as OH attached to aromatic rings. As shown in Table 1, the ratios of H/C and O/C of the demineralized coal chars decrease with increasing the preparation temperature, indicating the loss of hydrogen and oxygen during pyrolysis, which correlates well with the variations of their IR spectra.

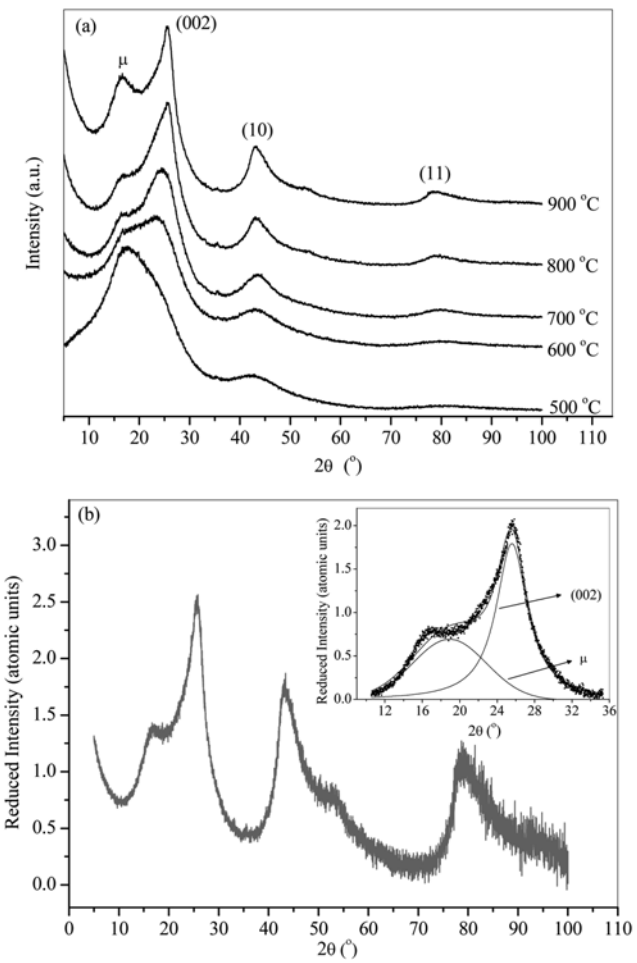

Fig. 2. XRD patterns of (a) PFR chars in original intensity and (b) the char pyrolyzed at 900 °C in reduced intensity.

2. XRD Characterization

Fig. 2(a) shows the XRD patterns of PFR chars. Three diffraction peaks were observed in all the char samples at $2\theta \approx 25^{\circ}$, 44° and 80°, corresponding to (002), (10) and (11) bands, respectively. The (002) band of carbon is attributed to the stacking structure of aromatic layers, while the (10) and (11) bands arise from the in-plane structure of the aromatics. In addition to the three aromatic peaks, a peak, designated as μ band, was also observed at $2\theta \approx 18.5^{\circ}$, which may be attributed to the packing of the structure such as aliphatic side chains or condensed saturated rings [16], or the adjacent chains of linear polymer [25]. Qualitatively, Fig. 2(a) shows that, with increasing the pyrolysis temperature, the (002) peak position shifts from 24.4° to 25.6°, closer to that of graphite (26.6°) and all the four peaks become more intense and sharper. In general, diffuse and broad bands in XRD patterns represent the existence of short-range order in the carbon structure, while sharp and narrow peaks correspond to highly crystalline with high degree of long-range order.

To obtain quantitative information of char structure from the XRD analysis, the approach of Alexander et al. [26] was followed to process the XRD raw data. The original intensity, as shown in Fig. 2(a), was normalized to electron units and then the incoherent scattering of carbon atom was subtracted from the normalized intensity. The reduced intensity was finally obtained by dividing the normalized intensity by coherent scattering of carbon atom. Because of the asymmetry of the (002) peak, the overlapped peaks were resolved into two peaks. The reduced intensity of the char pyrolyzed at 900 °C and its resolved m peak and (002) peak are presented in Fig. 2(b) as an example. Based on the reduced intensity, various structural parameters, including crystallite diameter L_a, average stacking height L_c and interlayer spacing d_{002}, can be derived. The classic Bragg's equation was used to calculate the interlayer spacing:

$$d_{002} = \lambda / 2\sin\theta_{002} \tag{3}$$

The crystallite diameter and average stacking height of the aromatic carbon sheets were estimated with Scherrer's formula:

$$L_c = \frac{0.9\lambda}{B_{002}\cos\theta_{002}}, \quad L_a = \frac{1.84\lambda}{B\cos\theta} \tag{4}$$

Based on Eq. (3) and Eq. (4), the values of the structural parameters were calculated for all the PFR char samples, and the results are summarized in Table 2.

Interlayer spacing d_{002} represents the extent of perfection in the periodicity of the stacking structure of aromatic layers and an estimation of a graphitization degree of carbon. A larger proportion of aliphatic chains bonded to graphene lamellae being piled up leads to larger value of d_{002} [27]; thus the loss of aliphatic structure, e.g., CH_2, reflected in IR spectra of Fig. 1(a) results in the decrease of d_{002} during pyrolysis. As shown in Table 2, the decrease of d_{002} and the increases of L_a and L_c with increasing the pyrolysis temperature suggest the development of stacking structure, increasing crystallite size as well as removal of defects and increasing order in char struc-

Table 2. XRD Crystallite parameters and Raman parameters of PFR chars

	XRD				Raman		
Sample	d/Å	L_c/Å	L_a(10)/Å	L_a(11)/Å	L_a(Raman)/Å	I_D/I_G	I_{1550}/I_G
PFR-500	3.64	6.1	19.6	11.9	-	-	-
PFR-600	3.61	8.5	19.5	12.3	13.7	3.2	0.398
PFR-700	3.55	10.7	26.2	17.5	16.4	2.7	0.344
PFR-800	3.48	15.4	31.0	17.9	18.1	2.4	0.281
PFR-900	3.48	19.9	29.9	18.1	22.6	1.9	0.305

- not analyzed

ture. Table 2 also shows that the values of L_a(10) appear much larger than that of L_a(11). Compared with (11) band, (10) band located more near to (002) band, it is likely to be affected by (002) band. Therefore the value of L_a(11) is believed to be more reliable than that of L_a(10) [28]. According to Emmerich [29], the increases of L_a and L_c with increasing pyrolysis temperature result from crystallite growth in-plane and coalescence of crystallites along the *c*-axis and *a*-axis. Heat treatment ranging from 500 to 900 °C in this study, owing to the evolution of volatile matter and the breakage of cross-linking bonds such as CH_2 bridge, the aromatic layers grow and coalesce between each other.

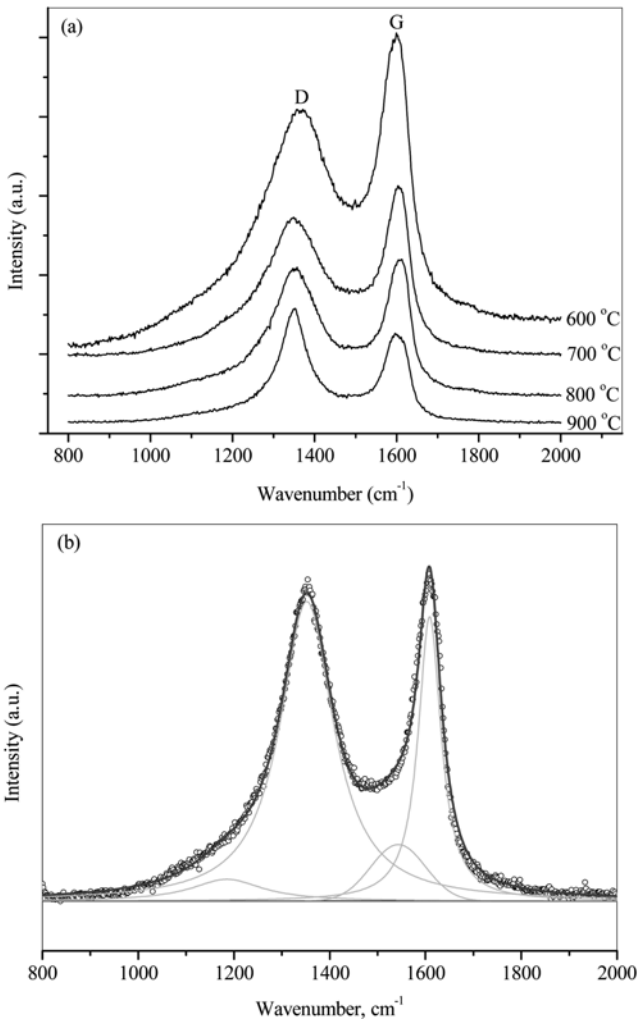

Fig. 3. (a) Typical Raman spectra of PFR chars and (b) curve-fitted Raman spectra of the char carbonized at 900 °C.

3. Raman Spectra Analysis

Typical Raman spectra of PFR chars pyrolyzed at the temperatures from 600 to 900 °C are presented in Fig. 3(a). They usually consist of four bands at ca. 1,150, 1,350, 1,550 and 1,600 cm^{-1}. For quantitative analysis, Raman spectra of PFR chars were fitted with 3 Lorentzian lines (1,150, 1,350, 1,600 cm^{-1}) and 1 Gaussian line (1,550 cm^{-1}). The resolved spectra of the char pyrolyzed at 900 °C are illustrated in Fig. 3(b) as an example. The 1,150 cm^{-1} band is attributed to sp^2-sp^3 bonds or C-C and C=C stretching vibrations of polyene-like structures [30,31]. The 1,350 cm^{-1} band represents defect structure (D band), corresponding to a graphitic breathing vibration mode with A_{1g} symmetry, and is attributed to the in-plane imperfections such as defects and heteroatoms [30,32]. The 1,550 cm^{-1} band originates from amorphous sp^2-bonded forms of carbon, such as organic molecules, fragments or functional groups or defects outside the plane of aromatic layers like tetrahedral carbons [33]. The 1,600 cm^{-1} band is a shifted graphite band (G band), which represents the stretching vibration mode with E_{2g} symmetry in the aromatic layers of the graphite crystalline. Fig. 3(a) shows that the bands of the Raman spectra of PFR chars sharpen up with increasing the pyrolysis temperature, indicating the ordering in the carbon structure.

Based on the de-convolution of the spectra, empirical parameters to define char structure can be obtained. The empirical formula proposed by Tuinstra and Koenig [34] was applied for evaluating L_a from Raman spectra:

$$L_a(\text{Raman})=44(I_D/I_G)^{-1} \quad (5)$$

The values of L_a(Raman), I_D/I_G and I_{1550}/I_G are also given in Table 2. The results in Table 2 indicate that L_a(Raman) increases with the pyrolysis temperature. Moreover, the values of L_a(Raman) show a good agreement with that of L_a(11) estimated from the XRD analysis. The values of I_D/I_G and I_{1550}/I_G decrease with increasing the pyrolysis temperature, which suggests that carbon structural rearrangement and the decrease of disorder. The variations of I_D/I_G and I_{1550}/I_G also result from the growth of stacking graphene layer and the loss of structural defects and imperfections acting as active sites.

4. Reactivity of PFR Char Towards NO

Fig. 4 shows the Arrhenius plots of PFR chars reacting with NO. At lower reaction temperature, the char pyrolyzed at 900 °C shows the lowest reactivity, while the char pyrolyzed at 700 °C shows the best reactivity at higher reaction temperature. There is a small difference among the reactivity of the char pyrolyzed at 500, 600 and 800 °C.

The reactive char surface on which the reduction of NO occurs consists of basal plane carbon atoms and active sites. The latter includes edge carbon atoms, phenolic OH, carboxyl, aromatic hydrogen, aliphatic hydrogen, nascent sites and inorganic species derived from mineral matter [14,35]. With increasing the pyrolysis temperature, IR spectrum of PFR chars shows a decrease of phenolic OH and aromatic hydrogen (see Fig. 1(a)). XRD and Raman spectra of PFR chars show a pronounced increase of the crystallite size (L_a, L_c) (see Table 2), which suggests an increase of the order in char structure. It is generally believed that an increase in crystallite structure order of coal char, resulting from severe heat treatment, causes a decrease in the ratio of active edge carbon atoms to inactive basal carbon atoms [14]. Therefore, the char pyrolyzed at 900 °C shows a weak reactivity at lower reaction temperature. However, the reactivity of the char pyrolyzed at 900 °C shows high values at higher reaction temperature instead, suggesting the PFR chars have a different ratio of reactive to non-reactive sites from coal char. The effect of pyrolysis temperature on the reactivity of PFR char is different from that of coal char, which is consistent with the results in Ref [5]. Similarly, the relative concentration of active sites on graphite was found to be different from that on activated carbon and carbon black since the graphite showed the highest reactivity towards NO, although it had the most ordered structure [19].

The apparent activation energy of NO-PFR char reaction was estimated and the results are given in Table 3. It can be seen in Table 3 that the apparent activation energy generally increases with increasing pyrolysis temperature.

It can be concluded that the gasification reactivity of PFR char is related to the micro-structure, but does not show regular variation with the pyrolysis temperature in the temperature range studied, although the carbon structure of PFR char becomes more ordered with increasing the pyrolysis temperature. Therefore, the effect of micro-structure on the reactivity of PFR char should be further examined in a wider pyrolysis temperature range.

5. Reactivity of Coal Char Towards NO

Fig. 5 shows the Arrhenius plots of coal chars and demineralized ones reacting with NO. Below 700 °C, char reactivity decreases markedly with the heat treatment temperature, while above 700 °C the reactivity experiences a sudden decline and shows a weak dependence on the pyrolysis temperature. This may be attributed to the possible diffusion limitation in the high temperature region. In addition, chars pyrolyzed at lower temperatures experience the reac-

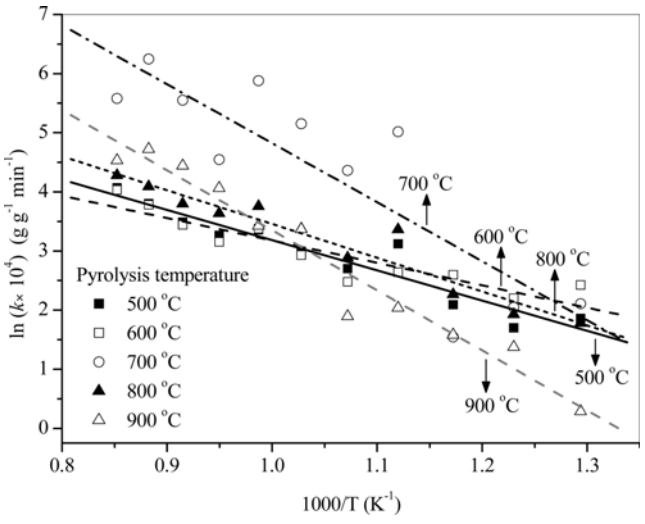

Fig. 4. Arrhenius plots of NO-PFR char reaction (The straight lines denote the linear fitting of the corresponding scatters).

Table 3. Apparent activation energy of NO-char reaction

Sample	Activation energy (kJ/mol)
PFR-500	43
PFR-600	32
PFR-700	83
PFR-800	48
PFR-900	85
SH-500	72
SH-700	90
SH-900	99
Dem-SH-500	66
Dem-SH-700	80
Dem-SH-900	94

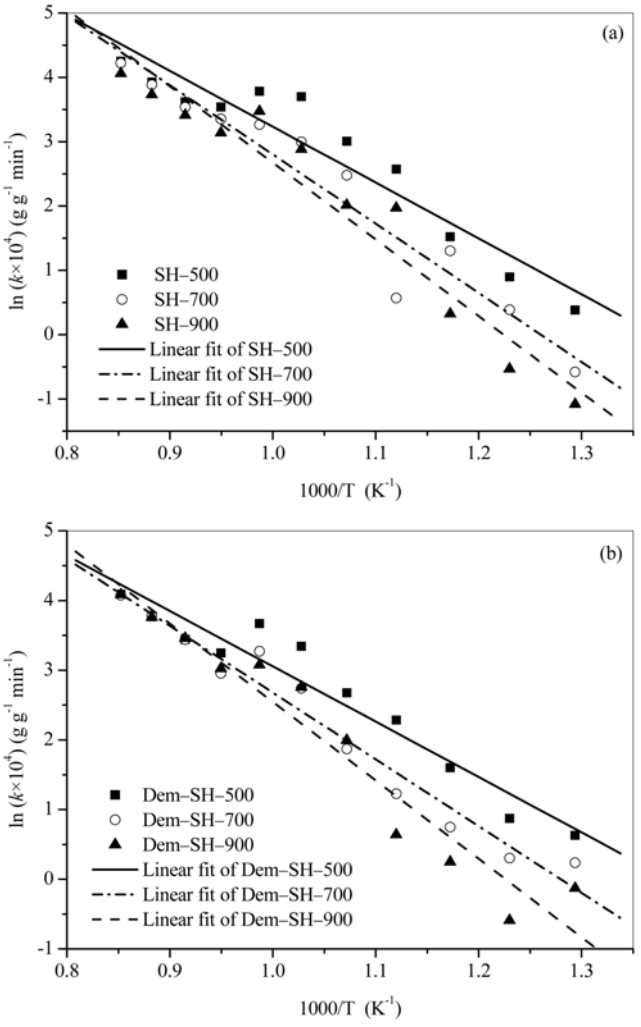

Fig. 5. Arrhenius plots of NO-coal char reaction: (a) raw coal char and (b) demineralized coal char.

tion temperature higher than the pyrolysis temperature, probably leading to a thermal deactivation similar to the effect of high temperature pyrolysis.

The functional groups in demineralized coal char vary significantly with increasing pyrolyzing temperature, as shown in Fig. 1(b). It is believed that heat treatment has an effect on the amount of active sites. According to Chan et al. [24], the decrease in the reactivity of char with hydrogen content could be related to the reduction in active sites. Since phenolic OH and aromatic hydrogen of coal char acting as active sites towards NO, their decreases with increasing pyrolysis temperature may be responsible for the decrease of reactivity. On the other hand, comparison of Fig. 5(a) with Fig. 5(b) indicates that mineral materials show a weak catalytic effect on NO-C reaction, although remarkable effects were reported in previous studies [9,10]. The calculated apparent activation energy of NO-coal char reaction is listed in Table 3. The results in Table 3 show that the apparent activation energy increases with increasing pyrolysis temperature, indicating lower reactivity of chars formed at higher pyrolysis temperatures particularly for lower temperature reaction.

CONCLUSIONS

Char samples were prepared by pyrolyzing two raw materials at various temperatures, which were then characterized by FTIR, XRD and Raman spectroscopy. The reactivity of char samples towards NO was measured in TGA. The pyrolysis temperature was found to have a significant impact on the micro-structure of both PFR chars and coal chars. The infrared spectra of both chars showed a decrease of OH groups and aromatic hydrogen. XRD and Raman spectroscopy of PFR char indicated increasing order in carbon structure during pyrolysis. The pyrolysis temperature showed a weak effect on the reactivity of PFR char but comparatively remarkable effect on that of coal char at lower reaction temperature. It could be confirmed that the micro-structure of PFR char and coal char showed different influence on the reactivity toward NO. Mineral matter in coal char played a weak catalytic role in the NO-char reaction.

ACKNOWLEDGMENT

The authors acknowledge the partial financial support of this work from the National Key Basic Research and Development Program of China (2006CB200302).

NOMENCLATURE

A : frequent factor [g g^{-1} min^{-1}]
B : full width at half maximum intensity of (10) peak or (11) peak [°]
B_{002} : full width at half maximum intensity of (002) peak [°]
C_{NO} : concentration of NO
d_{002} : interlayer spacing [Å]
E : apparent activation energy [kJ/mol]
I_D/I_G : peak area intensity ratio of D band to G band
I_{1500}/I_G: peak area intensity ratio of 1,550 cm^{-1} band to G band
k : reaction rate constant [g g^{-1} min^{-1}]
L_a : crystallite diameter [Å]
L_a(10), L_a(11) : L_a calculated from (10) and (11) peaks, respectively [Å]
L_a(Raman) : L_a calculated from Raman spectra [Å]
L_c : average stacking height [Å]
m : the mass of char (on dry ash free basis) at time t [g]
m_0 : the initial mass of char (on dry ash free basis) [g]
R : universal gas constant [J mol^{-1} K^{-1}]
r : global rate of gasification reaction [g g^{-1} min^{-1}]
t : reaction time [min]
T : reaction temperature [K]
X : carbon conversion

Greek Letters

θ : position of (10) peak or (11) peak [°]
θ_{002} : position of (002) peak [°]
λ : wavelength of the incident X-ray [Å]

Superscripts

n : reaction order

REFERENCES

1. W. Xu, H. Tong, C. Chen and X. Xu, *Korean J. Chem. Eng.*, **25**, 53 (2008).
2. P. Qiu, S. Wu, S. Sun, H. Liu, L. Yang and G. Wang, *Korean J. Chem. Eng.*, **24**, 683 (2007).
3. D. Klvana, J. Kirchnerova and C. Tofan, *Korean J. Chem. Eng.*, **16**, 470 (1999).
4. I. Aarna and E. M. Suuberg, *Fuel*, **76**, 475 (1997).
5. E. M. Suuberg and I. Aarna, *Kinetics and mechanism of NOx-char reduction*, Final Report DE-FG22-94PC94218 (1998).
6. Y. H. Li, G. Q. Lu and V. Rudolph, *Chem. Eng. Sci.*, **53**, 1 (1998).
7. A. Tomita, *Fuel Proc. Tech.*, **71**, 53 (2001).
8. Y.-C. Bak, *Korean J. Chem. Eng.*, **15**, 336 (1998).
9. Z. Zhao, J. Qiu, W. Li, H. Chen and B. Li, *Fuel*, **82**, 949 (2003).
10. M. J. Illan-Gomez, A. Linaes-Solano, L. R. Radovic and C. Salinas-Martinez de Lecea, *Energ. Fuel*, **10**, 158 (1996).
11. E. G. Garijo, A. D. Jensen and P. Glarborg, *Energ. Fuel.*, **17**, 1429 (2003).
12. Y. Takeuchi, K. Yanagisawa, Y. Tanaka and N. Tsuruoka, *Korean J. Chem. Eng.*, **14**, 377 (1997).
13. S.-J. Moon and S.-K. Ihm, *Korean J. Chem. Eng.*, **11**, 111 (1994).
14. L. R. Radovic, P. L. Walker and R. G. Jenkins, *Fuel*, **62**, 849 (1983).
15. O. Senneca, P. Russo, P. Salatino and S. Masi, *Carbon*, **35**, 141 (1997).
16. L. Lu, C. Kong, V Sahajwalla and D. Harris, *Fuel*, **81**, 1215 (2002).
17. A. Arenillas, F. Rubiera, J. J. Pis, J. M. Jones and A. Williams, *Fuel*, **78**, 1779 (1999).
18. A. Garcia-Garcia, M. J. Illan-Gomez, A. Linares-Solano and C. Salinas-Martinez de Lecea, *Fuel Proc. Tech.*, **61**, 289 (1999).
19. J. Yang, E. Sanchez-Cortezon, N. Pfander, U. Wild, G. Mestl, J. Find and R. Schlogl, *Carbon*, **38**, 2029 (2000).
20. P. C. Painter, M. M. Coleman, R. W. Snyder, O. Mahajan, M. Komatsu and P. L. Walker, *Appl. Spec.*, **35**, 106 (1981).
21. C.-L. Liu, W.-S. Dong, J.-R. Song and L. Liu, *Mat. Sci. Eng. A*, **459**, 347 (2007).
22. N. E. Cooke, O. M. Fuller and R. P. Gaikwad, *Fuel*, **65**, 1254 (1986).
23. J. Ibarra, R. Moliner and A. J. Bonet, *Fuel*, **73**, 918 (1994).

24. M. L. Chan, J. M. Jones, M. Pourkashanian and A. Williams, *Fuel*, **78**, 1539 (1999).
25. T.-H. Ko, W.-S. Kuo and Y.-H. Chang, *Polym. Composite*, **21**, 745 (2000).
26. L. E. Alexander and E. C. Sommer, *J. Phys. Chem*., **60**, 1646 (1956).
27. A. G. Alvarez, M. Martinez-Escandell, M. Molina-Sabio and F. Rodriguez-Reinoso, *Carbon*, **37**, 1627 (1999).
28. L. Lu, V. Sahajwalla and D. Harris, *Energ. Fuel*, **14**, 869 (2000).
29. F. G. Emmerich, *Carbon*, **33**, 1709 (1995).
30. C. Sheng, *Fuel*, **86**, 2316 (2007).
31. A. Sadezky, H. Muckenhuber, H. Grothe R. Niessner and U. Poschl, *Carbon*, **43**, 1731 (2005).
32. A. C. Ferrari and J.Robertson, *Phys. Rev. B*, **61**, 14095 (2000).
33. O. Beyssac, B. Goffe, J. P. Petitet, E. Froigneux, M. Moreau and J. N. Rouzaud, *Spectrochim. Acta. A*, **59**, 2267 (2003).
34. F. Tuinstra and J. L. Koenig, *J. Chem. Phys.*, **53**, 1126 (1970).
35. K. M. Thomas, *Fuel*, **76**, 457 (1997).